18th World IMACS / MODSIM Congress, Cairns, Australia 13-17 July 2009
http://mssanz.org.au/modsim09

Methods of assessing the performance of IPCC-AR4 models in simulating Australian rainfall teleconnections with Indo-Pacific climate drivers

Cai, W.[1], A. Sullivan[1], and T. Cowan[1]

[1] *CSIRO Marine and Atmospheric Research*
Email: wenju.cai@csiro.au

Abstract:

Significant improvements have been achieved in the simulation of Indo-Pacific variability, such as the India Ocean Dipole (IOD) and the El Niño-Southern Oscillation (ENSO) by models used in the Intergovernmental Panel on Climate Change Fourth Assessment Report (IPCC-AR4). In this paper, we discuss Australian rainfall teleconnections with these modes using 20th Century experiments from 23 IPCC-AR4 climate models. The results show that averaged over all models, the Australian rainfall teleconnection with ENSO is too weak over eastern Australia, and too strong over the northwest Western Australia. The latter is due to the well-known bias associated with the Pacific cold tongue, which extends too far west. Both the ENSO and IOD rainfall teleconnections vary strongly from one model to another, although the rainfall teleconnection with the IOD is more realistic compared with observations. Factors such as the amplitude of the simulated ENSO, the structure of the model cold tongue, and the signal to noise ratio in determining the teleconnections will be discussed.

Keywords: *Indo-Pacific variability, rainfall teleconnections, Indian Ocean Dipole.*

1. Introduction

There have been significant improvements in coupled general circulation models (GCMs) simulating El Niño-Southern Oscillation (ENSO) (Guilyardi, 2006), and the Indian Ocean Dipole (IOD) (Saji et al. 1999), with a realistic interplay between the thermocline depth, sea surface temperature (SST), precipitation, and zonal winds.

During El Niño, cooling in the west Pacific and warming in the central and eastern equatorial Pacific lead to more uniform SSTs. In association, a merger of the major convergence zones occurs: the Intertropical Convergence Zone (ITCZ) moves equatorward, while the South Pacific Convergence Zone (SPCZ) shifts northward, also the convergence zone over the west Pacific migrates to the east, where warm SST anomalies develop. This generates heavy rainfall in the central and eastern Pacific and droughts in Indonesia, the Phillippines, Hawaii, eastern Australia and the Fijian Islands. Like ENSO, the IOD has been shown to affect rainfall in many countries on the Indian Ocean rim and beyond (Behera et al. 2005). In a similar way, the associated rainfall variability reflects the movement of the convergence zones in the Indian Ocean sector, which can superimpose or counteract the impacts of ENSO. Through changes in the Walker Circulation and water vapour transport, a positive IOD (pIOD) event in the austral winter and spring causes drought in Indonesia and Australia (Ashok et al. 2003; Cai et al. 2005). Shi et al. (2008a) demonstrate that future Australian rainfall changes are a combined consequence of the long-term trend patterns associated with ENSO, the IOD, and the Southern Annular Mode. The result for Australia suggests that a realistic simulation of rainfall teleconnections could be important for reducing the uncertainty of climate projections. It is less clear how GCMs perform in terms of a rainfall teleconnection with these modes of variability, however as will be shown, the ENSO-rainfall and IOD-rainfall teleconnections vary vastly from model to model. We will focus on factors controlling the inter-model variations.

2. Model and data

We take 20th century climate simulation outputs, focusing on the period 1950-1999, from one experiment for each of the current 24 IPCC-AR4 GCMs. Outputs of rainfall and temperature are interpolated onto the same grid, detrended and then stratified into four seasons (December, January, February (DJF); March, April, May (MAM); June, July, August (JJA); September, October, November (SON)). In each GCM, an index for ENSO, Niño3.4 (average SST over 5°S-5°N, 170°W-120°W), is generated, and a correlation between the index and rainfall is calculated.

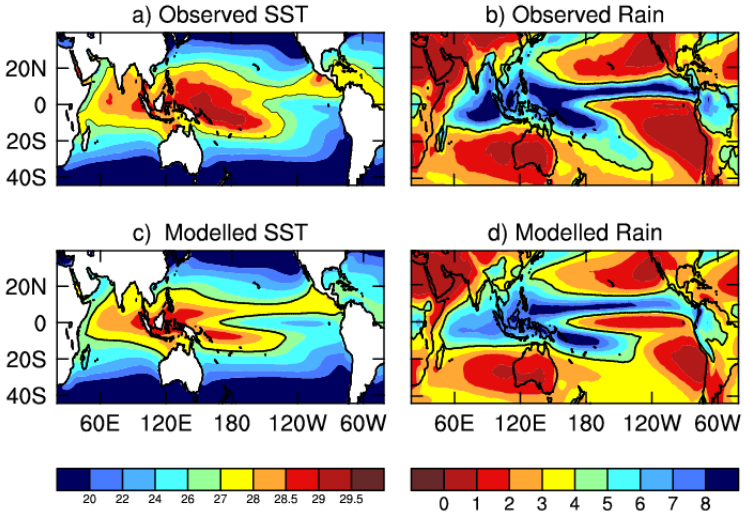

Figure 1. Climatology of annual-mean (a) SSTs (°C) and (b) rainfall (mm/day) from the observed compared with the all-model average in (c) and (d). The climatologies for (a), (c) and (d) are calculated across 1950-1999, whereas for (b) they are calculated over 1979-2006.

We also use available observational and reanalysis data:

- rainfall data from the Australian Bureau of Meteorology (BMRC) and NCEP.
- SST from Global Sea Ice and Sea Surface Temperature (HadISST) dataset (Rayner et al. 2003).

For reference, Figure 1 plots the annual mean Indo-Pacific SST and rainfall for the observed (Figs. 1a and 1b), and averaged over 24 models (Figs. 1c and 1d), for the period 1950-1999 (except for Fig. 1b, where the observed rainfall climatology is calculated over 1979-2006 from Climate Prediction Centre Merged Analysis of Precipitation (CMAP) (Xie and Arkin, 1997)).

The model SSTs feature the well-known bias of the equatorial Pacific cold tongue (Davey et al. 2002; Cai et al. 2003), which is too cold and extends too far into the west Pacific. As such, the model maximum SST, i.e., the Pacific warm pool, and the rising branch of the Walker Circulation are all located too far west. These features persist in all seasons (figures not shown). Most of the observed precipitation falls in the Indian Ocean, over the maritime continents, the equatorial west Pacific, and the Northern Hemisphere ITCZ, and the SPCZ (which tilts to the southeast). The model mean rainfall captures these features but produces the double ITCZ, which is another major tropical bias in the coupled GCMs (Lin 2007; Meehl et al. 2005). As such, low rainfall occurs along the equator and the model precipitation concentrates over Northern Hemisphere ITCZ and Southern Hemisphere SPCZ. As can be seen from Figure 1c, the narrowness of the warm pool and the strong zonal orientation of SST south of the equator are consistent with the rainfall pattern (Figure 1d). We will show that the unrealistic SST pattern has serious consequences for rainfall teleconnection.

3. ENSO-Rainfall teleconnection

We define the ENSO-rainfall teleconnection as the simultaneous correlation between Niño3.4 and grid-point rainfall anomalies. Correlation maps are constructed over each season for the observed and for each model (for Australian we use BMRC's high-quality rainfall data, elsewhere we use NCEP reanalysis).

3.1 Multi-model ensemble

Averaged over all 24 models, the correlation patterns between Niño3.4 and grid-point rainfall (Figure 2) show several realistic features. Firstly, there is generally higher equatorial and lower off-equatorial rainfall associated with an El Niño. Secondly, in JJA and SON, a lower rainfall anomaly over the eastern Indian Ocean associated with El Niño is generated, due to the fact some of the pIOD events occur coherently with El Niño, and vice-versa. Nevertheless,

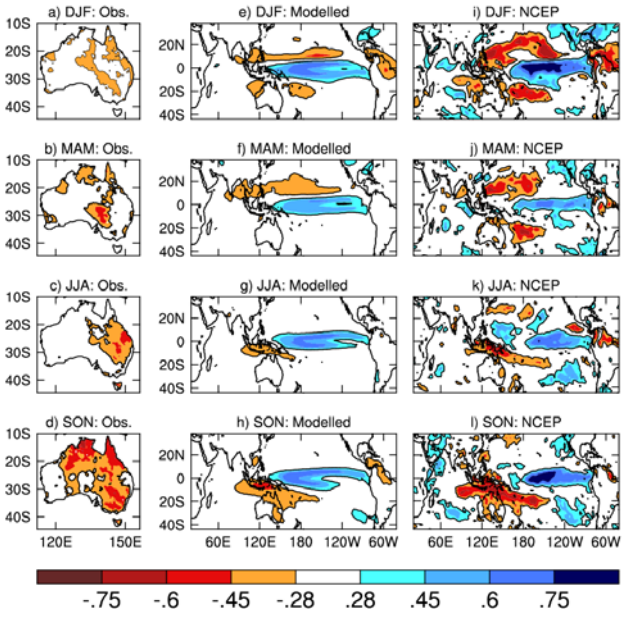

Figure 2. Correlation between Niño3.4 and grid-point Australian rainfall for (a) DJF, (b) MAM, (c) JJA, and (d) SON. (e)-(h) The same as (a)-(d) but averaged over 24 models. (i)-(l) The same as (a)-(d) but based on NCEP rainfall. A correlation with an absolute value greater than 0.28 is statistically significant at the 95% confidence level.

there is ample room for improvements. In the first case, the all-model average displays too low a correlation in most locations, leading to a correlation that is not significant at the 95% confidence level. For example, although many models produce an all-season rainfall reduction over eastern Australia during an El Niño, in the all-model average, this teleconnection is only significant in SON. Similarly, an observed El Niño is associated with a reduction in JJA rainfall over southern India and in DJF rainfall over tropical South America, but teleconnections over the two regions are simulated as not statistically significant in the all-model average. Positive correlations west of the international Dateline (meaning a rainfall increase during an El Niño) also extend too far west, leading to an overly strong teleconnection, particularly over western Papau New Guinea in DJF (Figure 2e). In association, poleward of the equatorial west Pacific, negative correlations in DJF and MAM (i.e., a reduction in rainfall associated with an El Niño) also extend too far west into the Indian Ocean, resulting in correlations over the north eastern Indian Ocean that are opposite to the observed.

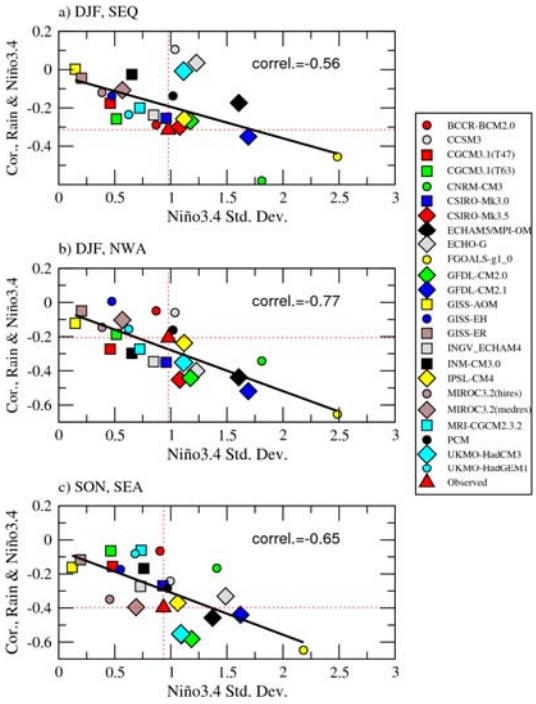

Figure 3. Scatter plot of inter-model variations of Niño3.4 correlations with rainfall against inter-model variations of the amplitude of ENSO (as measured by the one-standard deviation value of Niño3.4) for (a) DJF in the SEQ region (150°E-155°E, 20°S-30°S), (b) DJF in the NWA region (110°E-135°E, 10°S-30°S), and (c) SON in the SEA region (140E-155°E, 30°S-38°S). The slope and correlation of a linear fit are presented. Assuming each model is independent a correlation with an absolute value greater than 0.40 is statistically significant at the 95% confidence level.

3.2 Inter-model differences

For a given season, there are strong differences on a model to model basis, and often readers require information about the performance of individual models in their regions. To illustrate this point, we plot inter-model variations of the ENSO amplitude against inter-model variations of ENSO-rainfall teleconnection for several regions within continental Australia (Figure 3; see figure caption for region details). What is highlighted is a large number of models that have a relatively weak ENSO-rainfall teleconnection over south-east Queensland (SEQ) in DJF (Figure 3a), over south-east Australia (SEA) in SON (Figure. 3c), but too strong a teleconnection over north Western Australia (NWA) in DJF (Figure 3b).

In each of these plots, the correlation between inter-model variations of the ENSO-rainfall teleconnection and inter-model variations of the ENSO amplitude is shown. Assuming that each model is an independent sample, a correlation coefficient (labelled as 'correl' in Figure 3) with an absolute value greater than 0.4 indicates statistical significance at the 95% confidence level. In all cases selected here, such a significance level is achieved. Thus the control on the ENSO-rainfall teleconnection by the ENSO amplitude is systematic, highlighting the importance of realistically simulating this attribute.

In models with a stronger ENSO amplitude, the rainfall variability is more likely to be overwhelmed by ENSO-induced signals. We define "signal" as the standard deviation associated with the Niño3.4 (determined from a linear regression onto the Niño3.4 index), and "noise" as the standard deviation of the residual after removing ENSO-induced rainfall signals. What we find is that the greater the ENSO amplitude, the greater the ratio of "signals to noise." It follows that the ratio provides a stronger control over the ENSO-rainfall teleconnection than the ENSO amplitude. This is because it is a description of not only the ENSO-induced rainfall signals, but also its relative strength to stochastic noise. The relationship between the inter-model variations of the ratio and the inter-model variations of the ENSO-rainfall teleconnection across Australia is strong, and has a correlation greater than 0.9, statistically significant at the 99% confidence level (figure not shown).

4. IOD-rainfall teleconnection

4.1 Model IOD and its index

Our IOD index is defined as the leading component of SST anomalies in the Indian Ocean between 20°S and 20°N. Empirical Orthogonal Function (EOF) analysis was carried out for each season and for each model. In our EOF analysis, the variance is expressed in the EOF pattern, the principal component being scaled to unity, i.e., with a standard deviation of one.

The majority of models feature an IOD pattern that starts to develop in JJA with cooler SSTs in the east, and peaks in SON, as in the observed. Saji et al. (2006) show that this results from a GCMs' ability to simulate the seasonal cycle of the Indian Ocean, in which observed upwelling-favourable winds are generated off the Sumatra-Java coast in June-October, essential for an IOD to develop (Xie et al. 2002).

4.2 The IOD-rainfall teleconnection

Maps of the IOD-rainfall teleconnection for the JJA and SON are constructed through correlation analysis between the IOD index with grid-point rainfall anomalies. Figure 11 shows maps from the observed (Figures 4a and 4b), averaged over all models (Figures 4c and 4d), and based on NCEP (Figures 4e and 4f). In JJA, the teleconnection is generally weak; this is the case over much of SEA (Figure 4, top panels). In SON (Figures 4, lower panels), a pIOD is associated with a decrease in rainfall over SEA, the Sumatra-Java region, and east Africa. Compared with the teleconnection pattern from the NCEP reanalysis, the modelled teleconnection over the eastern Indian Ocean is realistic in size (Figures 4d and 4f), but too weak over SEA (Figures 4b and 4d).

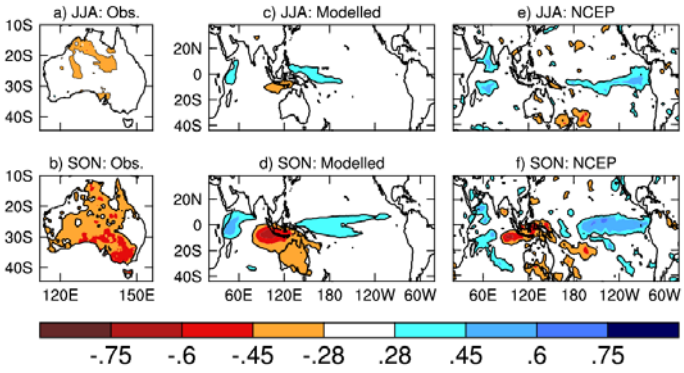

Figure 4. Correlation between an IOD index (time series of the Indian Ocean SST EOF1 taken from HadISST) and grid-point Australian rainfall in (a) JJA, and (b) SON. (c)-(d) The same as (a)-(b) but for a 24 model ensemble average. (e)-(f) The same as (a)-(b) but based on NCEP rainfall (with HadISST). Only absolute values greater than 0.28 are plotted, which are statistically significant at the 95% confidence level.

4.3 Inter-model differences

Similar to the ENSO-rainfall teleconnection, there are strong inter-model differences with respect to the IOD-rainfall teleconnection. Although for a given location the strength of the teleconnection differs vastly, a clear relationship of a stronger IOD associated with a stronger IOD-rainfall teleconnection emerges (figure not shown). Similar to the process associated with ENSO, the stronger the IOD amplitude and the IOD signal relative to the noise, the better the IOD influence on rainfall is manifested. The control on inter-model variations of the IOD-rainfall teleconnections by inter-model variations of the IOD rainfall signal to noise ratio is rather strong, with a correlation close to or above 0.9 (not shown).

5. Conclusions

In recent years, there have been significant improvements in the simulation of ENSO and the IOD in terms of amplitude and frequencies. These modes of the Indo-Pacific variability affect global rainfall, particularly throughout the tropical latitudes. Given that climate change and subsequent impacts tend to manifest through existing modes of variability, future rainfall changes rely heavily on the ability of climate models to simulate the strength and spatial pattern of rainfall teleconnections.

We show that the strength of a teleconnection for a given location is overwhelmingly controlled by the amplitude of ENSO, even more strongly by its signal strength relative to stochastic noise, highlighting the importance of realistically simulating these parameters. The deficiencies in the spatial pattern of the ENSO-rainfall teleconnection are mostly attributable to errors in the climatological SST and ENSO SST anomaly pattern. The ENSO-rainfall teleconnection mainly arises from the movement of convergence zones from their mean positions. The well-known equatorial Pacific SST climatology and ENSO cold tongue anomaly biases lead to many systematic errors.

Similarly, the IOD-rainfall teleconnection strengthens with the amplitude of the IOD, and its relative strength to that of noise. In general, there is no systematic linkage between the ENSO amplitude and IOD-ENSO coherence. Indeed, the majority of models produce an ENSO-IOD relationship lower than the observed, supporting the notion that the Indian Ocean has variability beyond ENSO and that ENSO is not the only trigger of IOD events.

Acknowledgement
The authors are supported in part by the Department of Climate Change, and in part by the Queensland Urban Water Security Alliance. In addition, we acknowledge the outstanding work undertaken by the many international modeling groups who provided their numerous model experiments for the Program for Climate Model Diagnosis and Intercomparison (PCMDI). For more details on model data or documentation, readers are referred to the PCMDI Web site (http://www-pcmdi.llnl.gov)

References

Ashok, K., Z. Guan, and T. Yamagata, 2003: Influence of the Indian Ocean Dipole on the Australian winter rainfall. *Geophys. Res. Lett.*, **30,** 1821, doi:10.1029/2003GL017926.

Behera, S. K., J. J. Luo, S. Masson, P. Delecluse, S. Gualdi, and A. Navarra, 2005: Paramount impact of the Indian Ocean dipole on the east African short rains: A CGCM study. *J. Climate*, **18**, 4514–4530.

Cai, W., M. A. Collier, H. B. Gordon, and L. J. Waterman, 2003: Strong ENSO variability and a Super-ENSO pair in the CSIRO mark 3 coupled climate model. *Mon. Wea. Rev.*, **131**, 1189–1210.

Cai, W., H. H. Hendon, and G. Meyers, 2005: Indian Ocean dipole-like variability in the CSIRO Mark 3 coupled climate model. *J. Climate*, **18**, 1449–1468.

Davey, M. K., and Coauthors, 2002: STOIC: A study of coupled model climatology and variability in tropical ocean regions. *Climate Dyn.*, **18**, 403–420.

Guilyardi, E, 2006: El Niño–mean state–seasonal cycle interactions in a multi-model ensemble. *Climate Dyn.,* **26:** 329–348 DOI 10.1007/s00382-005-0084-6.

Lin J. L. 2007: The Double-ITCZ Problem in IPCC AR4 Coupled GCMs: Ocean-Atmosphere Feedback Analysis. *J. Climate*, **20**, 4497–4525.

Meehl, G. A., C. Covey, B. McAvaney, M. Latif and R. J. Stouffer. 2005: OVERVIEW OF THE COUPLED MODEL INTERCOMPARISON PROJECT. *Bull. Amer. Meteor. Soc.*, **86,** 89–93.

Rayner, N.A., and Coauthors, 2003: Global analyses of sea surface temperature, sea ice, and night marine air temperature since the late nineteenth century. *J. Geophys. Res.*, 108(D14) 4407, doi:10.1029/2002JD002670.

Saji, N.H., B. N. Goswami, P. N. Vinayachandran, and T. Yamagata, 1999: A dipole mode in the tropical Indian Ocean. *Nature*, **401,** 360–363.

Saji, N.H., S. -P. Xie, and T. Yamagata, 2006: Tropical Indian Ocean Variability in the IPCC Twentieth-Century Climate Simulations, *J. Climate*, **19**, 4397–4417.

Shi, G., J. Ribbe, W. Cai, and T. Cowan, 2008: An interpretation of Australian rainfall projections. *Geophys. Res. Lett.*, L02702, doi:10.1029/2007GL032436.

Shinoda, T., H. H. Hendon, and M. A. Alexander, 2004: Surface and subsurface dipole variability in the Indian Ocean and its relation with ENSO. *Deep-Sea Res.*, **51,** 619–635.

Xie, P., and P.A. Arkin, 1997: Global Precipitation: A 17-Year Monthly Analysis Based on Gauge Observations, Satellite Estimates, and Numerical Model Outputs. *Bull. Amer. Meteor. Soc.*, **78**, 2539–2558.

Xie, S.-P., H. Annamalai, F. A. Schott, and J. P. McCreary, 2002: Structure and mechanisms of south Indian Ocean climate variability. *J. Climate*, **15,** 864–878.